Photochemistry and Spectroscopy
https://www.sciltp.com/journals/ps

Article

Tunable UV Photoexcitation of Carbon Atomic Wires: Investigating the Roles of Chain Length, Termination Groups, and Environment

Simone Melesi [1], Pietro Marabotti [1,2], Barbara Rossi [3], Valeria Russo [1], Andrea Li Bassi [1], Chiara Bertarelli [4], Carlo E. Bottani [1] and Carlo S. Casari [1,*]

[1] Department of Energy, Micro and Nanostructured Materials Laboratory-NanoLab, Energy, Politecnico di Milano, Via Ponzio 34/3, 20133 Milano, Italy
[2] Institut für Physik, Humboldt-Universität zu Berlin, Newtonstraße 15, 12489 Berlin, Germany
[3] Elettra Sincrotrone Trieste, S.S. 114 km 163.5 Basovizza, 34149 Trieste, Italy
[4] Department of Chemistry, Materials and Chemical Engineering "Giulio Natta", Politecnico di Milano Piazza Leonardo da Vinci 32, 20133 Milano, Italy
* Correspondence: carlo.casari@polimi.it

How To Cite: Melesi, S.; Marabotti, P.; Rossi, B.; et al. Tunable UV Photoexcitation of Carbon Atomic Wires: Investigating the Roles of Chain Length, Termination Groups, and Environment. *Photochemistry and Spectroscopy* **2026**, *2*(1), 3. https://doi.org/10.53941/ps.2026.100003

Received: 31 October 2025
Revised: 1 December 2025
Accepted: 2 December 2025
Published: 20 January 2026

Abstract: Carbon atomic wires (CAWs), linear one-dimensional carbon nanostructures, are attracting increasing attention in materials science due to their remarkable electrical, mechanical, optical, and transport properties, which make them promising candidates for being the next generation supercapacitors, batteries, hydrogen storage, organic semiconductors, and active optical elements. However, their intrinsic instability currently hinders their practical implementation. Previous studies have shown that CAWs mainly degrade through crosslinking interactions, exposure to high temperatures, hydrogenation and oxidation. Furthermore, a clear relationship between the wire structure, solvent polarity, and stability has been observed, with longer wires and more polar solvents reducing CAWs stability, while terminal groups strongly influence the degradation processes. Despite this, the photodegradation kinetics has not yet been fully and systematically investigated. Gaining such understanding is of fundamental importance for the rational design of CAWs-based materials for optoelectronic applications where light exposure is inevitable. In this work, we introduce a synchrotron-based approach that enables precise photoexcitation of CAWs with different chemical structures, tuned in resonance with their characteristic absorption vibronic peaks in the UV. This UV resonance Raman approach allows real-time monitoring of photodegradation directly through the time evolution of Raman spectra of each wire. We compare the photostability in different environments (i.e., acetonitrile, water, and aqueous colloidal silver nanoparticle dispersions), focusing on the role of two key structural parameters—sp-carbon chain length and terminal functional groups—in controlling the stabilization of these systems.

Keywords: carbon; polyynes; photodegradation; nanoparticles; UV resonance Raman spectroscopy; synchrotron

1. Introduction

Carbynes represent the ideal one-dimensional carbon nanocrystal, defined as an infinite linear chain with a one-atom cross-section composed exclusively of sp-hybridized carbon atoms [1,2]. Depending on the bond arrangement along the sp-carbon chain, carbynes are classified as polyynes (alternating single and triple bonds and

presenting a semiconducting behavior) or cumulenes (consecutive double bonds with a metallic behavior) [1,2]. The finite analogues of carbyne, i.e., carbon atomic wires (CAWs), are linear sp-carbon chains of finite length terminated by various functional groups. CAWs are attracting growing interest because of their remarkable electrical, mechanical, and optical properties, which make them appealing candidates for applications in capacitors [3,4], batteries [5], hydrogen storage [6,7], field-effect transistors (FETs) [8], organic electronics [9], molecular barcoding [10], and more. A key advantage is their high tunability: both the sp-carbon chain length (i.e., number of sp-carbon atoms) and the terminal functional groups strongly influence their optoelectronic response [11–16] and overall properties, opening a broad spectrum of potential applications.

Polyynes (in this context defined as CAWs with alternating structure) can be produced through either chemical [17–21] or physical methods [22–25]. Among the latter, pulsed laser ablation in liquid (PLAL) is one of the most widely used techniques, offering a cost-effective route to polyynes of various lengths and terminations [26–36]. However, PLAL yields only low-concentration polydispersions with poor control over chemical structure (i.e., sp-carbon chain presenting various lengths and termination groups). High-performance liquid chromatography (HPLC) can then be employed to separate polyynes by size and termination, enabling the isolation of purified monodispersed samples composed solely of polyynes with the same structure [26,28,32,37–39].

Despite their potential, the main limitation of polyynes is their intrinsic instability. One of the main degradation pathways is crosslinking, where sp-carbon chains interact with each other to form more stable sp^2 carbon networks [1,40]. Other degradation processes include hydrogenation (in the presence of hydrogen atoms) [41,42], oxidation (favored by oxygen or ozone) [43–45], and thermal degradation [40,43–45]. Longer chains are generally more prone to degradation [32,42], while termination groups critically influence the likelihood of degradation [15,32,42]. Polyyne stability is also influenced by the solvent in which they are synthesized or stored. Organic solvents confer much greater stability than water, due to the high solubility of polyynes in nonpolar environments, which inhibits aggregation and crosslinking [32]. Several strategies have been proposed to enhance stability, such as adopting bulky terminal groups to hinder intermolecular interactions, thus reducing the probability of crosslinking [21,46–50], or encapsulation within solid matrices (e.g., SiO_2 gel, carbon nanotubes, polymers) [15,33,51–56]. Stabilization can also be achieved through interactions with other nanostructures, such as metal nanoparticles [33,55–57].

In contrast, only a few studies have explored the excited states of polyynes [58] and their behavior under photoexcitation [15,43,59], showing that exposure to UV light induces photolysis and structural degradation. However, these studies present limitations. Continuous lamps covering 222–580 nm irradiate different polyynes with unequal power distributions across wavelengths, leading to non-uniform excitation depending on the absorption frequencies of different polyynes [43,59]. Monochromatic sources have also been employed [15,43,59], but in most cases their emission does not match the vibronic absorption peaks of polyynes, leading to inefficient excitation and making comparisons between different polyyne lengths unreliable, as the excitation efficiency depends on how close the vibronic peaks are to the source wavelength. In both cases, a systematic comparison among different carbon atomic wires is not possible, as different polyynes are exposed to non-identical experimental conditions. Lastly, some of these studies [43,59] investigated non-purified polyyne polydispersions, where polyynes with different structures and synthesis by-products coexist at varying concentrations, preventing a direct comparison among them and additionally introducing uncontrolled interactions both between different polyynes and with synthesis by-products.

In this work, we investigate the time-dependent photodegradation of size- and termination-selected polyynes produced via PLAL and separated via HPLC, focusing on sp-carbon chains of different lengths (HC_nH, n = 8, 10, 12) and terminations (HC_8X, X = H, Cl) to understand the role of these two structural parameters on their photostability mechanism. Our systematic approach employs highly tunable (1 nm resolution) monochromatic synchrotron radiation, enabling precise excitation of each polyyne at its main vibronic absorption peak under constant irradiation power. This ensures a rigorous comparison of photodegradation across polyynes with different structures. Moreover, synchrotron excitation in resonance with absorption peaks enables simultaneous characterization by UV resonance Raman (UVRR) spectroscopy, allowing us to monitor photodegradation directly through the evolution of the Raman spectra. Finally, to account for environmental effects and to evaluate the stabilization induced by metal nanoparticles, we investigated the influence of the solvent and nanostructure interactions by comparing the photostability of polyynes in pristine solutions, when mixed with pure distilled water, and mixed with aqueous dispersions of silver nanoparticles (AgNPs).

2. Materials and Methods

2.1. Materials

Acetonitrile (MeCN, HPLC plus gradient grade) and dichloromethane (DCM, HPLC grade, stabilized with amylene, ≥99.9% purity) were purchased from Carlo Erba Reagents (Milano (MI), Italy). Silver nitrate ($AgNO_3$, puriss. p.a., ACS reagent, ≥99.8%) was obtained from Sigma-Aldrich (Burlington, Massachusetts, MA, USA), and sodium citrate tribasic dihydrate (puriss. p.a., ACS, ≥99.0%) from Fluka Analytical (Buchs (SG), Switzerland). Deionized Milli-Q water (resistivity 0.055 μS) was produced directly in our laboratory.

2.2. Polyynes and Silver Nanoparticles Production

Monodispersed solutions of polyynes (i.e., size- and termination-selected) with different sp-carbon chain lengths (HC_nH, n = 8, 10, 12) and terminations (HC_8X, X = H, Cl) were prepared by pulsed laser ablation in liquid (PLAL), followed by high-performance liquid chromatography (HPLC) separation. Polydisperse polyyne mixtures were obtained by ablating a graphite target (99.99% purity, Testbourne Ltd., Basingstoke, UK) immersed in 5 mL of solvent (MeCN for X = H and DCM for X = Cl) for 30 min using the first harmonic (1064 nm) of an ns-pulsed Nd:YAG laser (Quantel Q-Smart 850). The laser pulse duration was 5–7 ns, with a repetition rate of 10 Hz. The beam was focused onto the graphite surface with a 200 mm focal length lens, yielding an estimated energy fluence of 2.71 J cm^{-2} and a spot radius of 0.766 mm.

The resulting polydisperse polyyne solutions were separated by sp-carbon chain length and termination using reverse-phase HPLC (Shimadzu Prominence UFLC), equipped with a photodiode array (DAD) UV-Vis spectrometer, an FRC-10A fraction collector, and a Luna 3 μm C18 semi-preparative column. Monodisperse polyynes were isolated by gradient elution with a mixture of acetonitrile and water as the mobile phase. All the CAWs investigated in this work elute at an acetonitrile concentration higher than that of water. Residual water is further removed using $MgSO_4$ as a drying agent. As a result, size- and termination-selected CAWs can be considered dissolved in nearly 100% acetonitrile. Hereafter, the as-prepared size- and termination- HPLC-isolated solutions are referred to as pristine solutions (concentration of 2.29×10^{-5} M, 1.45×10^{-5} M, 6.41×10^{-6} M, and 1.83×10^{-5} M for HC_8H, $HC_{10}H$, $HC_{12}H$, and HC_8Cl, respectively).

An aqueous colloidal dispersion of silver nanoparticles (AgNPs) was synthesized according to the Lee–Meisel method [60]. From their UV-Vis absorption spectra (see SI), the AgNPs displayed a plasmonic peak centered at 439 nm, which corresponds to an average diameter of approximately 75 nm, calculated according to the equation reported by Amirjani et al. [61]. Size- and termination-selected pristine polyynes solutions were subsequently mixed (1:1 *V*/*V*) with either pure distilled water or the AgNPs dispersion.

2.3. UV-Vis Spectroscopy

UV-Vis spectra of polyynes and AgNPs were recorded with a Shimadzu UV-1800 UV/visible scanning spectrophotometer, operating in the 190–1100 nm range. Measurements were carried out using quartz cuvettes with a 10 mm optical path and a spectral sampling interval of 0.2 nm. To avoid detector saturation, the AgNPs dispersion was diluted tenfold with pure distilled water before measurement.

2.4. UV Resonance Raman Spectroscopy and Photodegradation Experiments

UV resonance Raman (UVRR) spectra were acquired at the IUVS beamline of the Elettra Sincrotrone Trieste (Trieste, Italy) using its dedicated synchrotron-based UVRR setup [62]. Excitation wavelengths were selected to match the main vibronic peak of each polyyne (226, 251, 272, and 233 nm for HC_8H, $HC_{10}H$, $HC_{12}H$, and HC_8Cl, respectively; see Figure 1a) by finely adjusting the undulator gap aperture to tune the synchrotron radiation energy. The emitted light was subsequently monochromatized with a 750 mm focal length monochromator (Acton SP2750, Princeton Instruments, Trenton, NJ, USA) equipped with a 3600 grooves/mm holographic grating. Excitation beyond 272 nm or below 200 nm was not possible due to the physical limits of the undulator gap and the optical elements of the monochromator. The power delivered to the sample was kept constant at 4 μW using appropriate filters. The UVRR spectra were collected in back-scattering geometry using a 75 cm spectrograph (Trivista 557, Princeton Instruments) equipped with holographic gratings with 1800 and 3600 grooves/mm and with a UV-enhanced CCD camera. Calibration was performed with the Raman peaks of cyclohexane. The spectral resolution was set at $\frac{spectral\ range}{1340}$ cm^{-1}/pixel, depending on the excitation wavelength (i.e., 2.5 cm^{-1}/pixel at 226 nm, 1.9 cm^{-1}/pixel at 251 nm, 1.6 cm^{-1}/pixel at 272 nm, and 2.3 cm^{-1}/pixel at 233 nm).

Photodegradation experiments were carried out exciting the polyynes by using the same synchrotron photon source, which simultaneously served as the excitation for UVRR acquisition. This hybrid approach enabled direct monitoring of polyyne photodegradation through the time-dependent evolution of their characteristic Raman peaks.

3. Results and Discussion

Polyynes have been investigated using a combination of UV-Vis absorption spectroscopy and Raman spectroscopy. Indeed, UV-Vis absorption spectra of polyynes exhibit a series of characteristic absorption vibronic peaks, whose positions depend on sp-carbon chain length and termination functional groups [16,32,63–66]. Similarly, polyynes Raman spectra display an intense and characteristic mode, described by the effective conjugation coordinate (ECC) model, which corresponds to an in-phase stretching of all the CC bonds along the sp-carbon chain [1,11,67,68]. This ECC mode lies in the 1800–2300 cm^{-1} range, a region free of Raman-active modes for other carbon allotropes, thus serving as an unambiguous fingerprint of *sp*-hybridized carbon nanomaterials [1,2]. The ECC frequency is also sensitive to sp-carbon chain length and termination groups [15,16,65,67,69]. Consequently, the combined analysis of vibronic peak positions and ECC mode frequency provides valuable information on the chemical structure of polyynes and can be used to monitor the time evolution of these species. However, PLAL-produced polyynes often fall below the Raman detection limit. Resonance enhancement, achieved by tuning the UV excitation to a polyynic vibronic absorption peak, can enhance the Raman signal up to six orders of magnitude [70,71], enabling the detection of even very low-concentration (in the order of 10^{-5}–10^{-6} M) polyynes samples [36,72,73]

In this work, different solutions of length- and termination-selected polyynes were irradiated with monochromatic light at the IUVS beamline of the Elettra Sincrotrone Trieste. To enable a reliable comparison among the various polyynes, each sample was excited at its main vibronic absorption peak (see Materials and Methods and Figure 1a), while keeping the delivered power (i.e., 4 µW) constant. Under these resonant conditions, synchrotron radiation was employed to perform UV resonant Raman (UVRR) spectroscopy, yielding strong Raman signals even from these low-concentrated (≈10^{-5} M–10^{-6} M, see Materials and Methods) polyyne solutions. Examples of UVRR spectra for each polyyne are shown in Figure 1b and in Figure S1, highlighting the main characteristic Raman peaks of polyynes (i.e., the ECC mode [1,2,11,67,68] and a secondary weaker mode, called β mode [67,68] as well as the CN stretching vibration of the solvent (i.e., acetonitrile, MeCN).

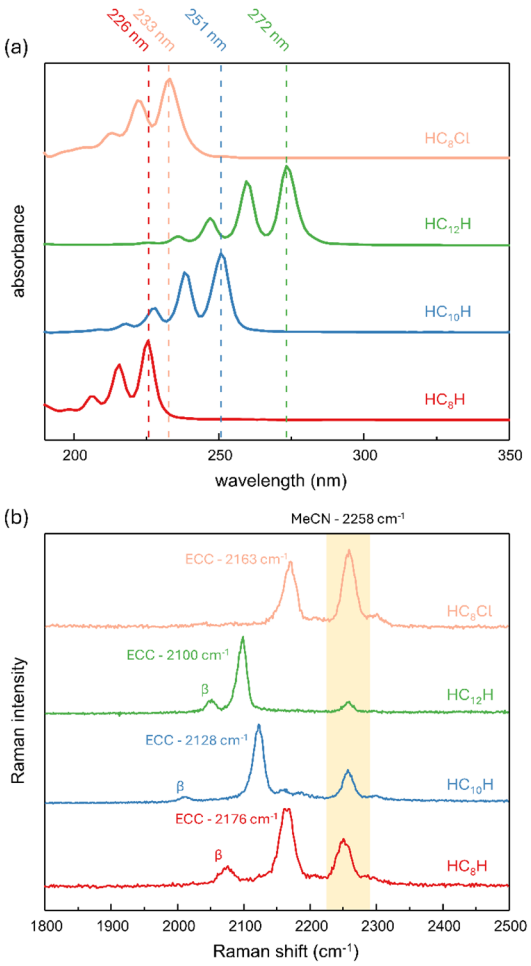

Figure 1. (**a**) UV–Vis spectra of all polyynes investigated in this work. Dashed lines indicate the synchrotron excitation wavelengths used to perform UVRR for each polyyne. HC_8H, $HC_{10}H$, $HC_{12}H$, and HC_8Cl were excited

at 226, 251, 272, and 233 nm, respectively, corresponding to their first vibronic peak. (**b**) UVRR spectra of polyynes in solutions. The frequency of the ECC mode for each polyyne is reported, together with their β mode (when visible) and the CN stretching frequency of the solvent (acetonitrile, MeCN) highlighted in light yellow. The full Raman spectra are reported in Figure S1.

Photodegradation was investigated by monitoring the time-dependent decrease of the ECC for each investigated polyyne. An example of the time evolution of the UVRR spectra of polyynes is shown in Figures 2a and S2, together with the corresponding time evolution of the area of the ECC and MeCN peaks (Figure 2b), evaluated by fitting each spectrum using a Lorentzian model and considering the area of each fitted peak. As previously reported in the literature [36,74–76], correct interpretation of UVRR spectra requires accounting for self-absorption (SA) phenomena: under resonance, polyyne solutions absorb part of both the incident and the scattered photons, thereby reducing the measured Raman intensity. Since irradiation progressively degrades polyynes and decreases their concentration, photon absorption and the associated SA cannot be considered constant throughout the experiment. The data presented here already take into account these variations in SA, and the model used for correcting the raw spectra is described in the SI.

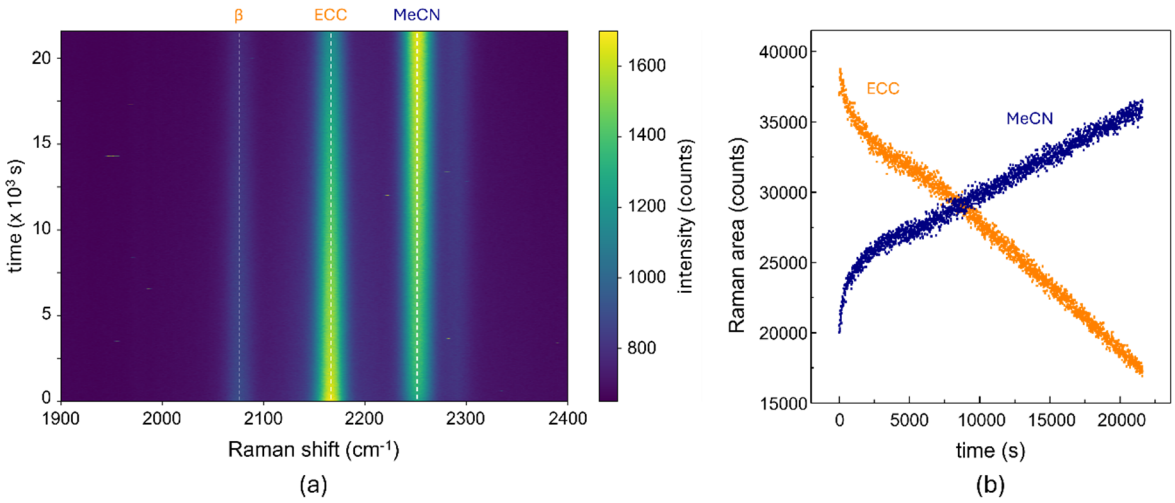

Figure 2. (**a**) Time evolution of the UVRR spectra of HC_8H. The ECC, the β mode, and the solvent (MeCN) Raman peaks are indicated with dashed lines. (**b**) Corresponding time evolution before the SA-correction of the area of the ECC and MeCN peaks shown in (**a**).

The role of sp-carbon chain length in the photodegradation behavior of these systems was assessed by comparing hydrogen-capped polyynes of different lengths (HC_nH, with n = 8, 10, and 12). Figure 3a shows the time evolution of the ECC Raman mode area for size-selected polyynes obtained with HPLC separation (labeled as pristine samples). Interestingly, shorter polyynes (HC_8H) display lower photostability than the longer ones ($HC_{10}H$ and $HC_{12}H$). Specifically, the percentages of non-photodegraded polyynes after irradiation (calculated as the ratio between the final ECC values after 6 h of irradiation and their corresponding initial ones) are 27, 49, and 95% for HC_8H, $HC_{10}H$, and $HC_{12}H$, respectively. This non-trivial trend is the opposite of what has been previously reported for polyyne stability in solutions (without photoexcitation), where stability decreases with increasing sp-carbon chain length [42,77]. Moreover, the literature reports that the molar extinction coefficient of polyynes increases with the length of the sp-carbon chain [78]. This implies that, if the degradation pathway is mainly photo-activated, longer chains will absorb more photons and, consequently, undergo greater photodegradation, contrary to what is observed. One possible explanation for this unexpected trend could be related to the different concentrations of polyynes with different lengths. Shorter chains are produced in larger amounts by PLAL and, during HPLC separation, they experience lower dilution [27,37], resulting in monodispersed solutions with concentrations decreasing as the sp-carbon chain length increases (see Figure S3 and Materials and Methods). Higher concentrations can favor crosslinking and other secondary photo-induced mechanisms (e.g., excimer formation or intermolecular excited-state reactions, which can lead to crosslinking [79,80]) that accelerate photodegradation, which would make short polyynes less stable under irradiation. To test this hypothesis, the same experiment was repeated after diluting all pristine monodisperse solutions to 5×10^{-6} M, close to the value of the $HC_{12}H$ pristine concentration, the least concentrated sample. The results presented in Figure 3b clearly show that an unexpected trend persists even at equal concentration, with HC_8H remaining the least stable species under

photoirradiation (76% of non-photodegraded polyynes after 6 h of photoirradiation), while $HC_{10}H$, of intermediate length, is the most stable (87 and 80%, for $HC_{10}H$ and $HC_{12}H$, respectively). The consistently lower photostability of HC_8H rules out concentration-related effects (e.g., crosslinking) as the primary cause of this non-trivial behavior. Nevertheless, the interplay between concentration and sp-carbon chain length is evident in Figure 3c, which shows the percentage change of the ECC Raman intensity (after six hours of irradiation) when going from high concentration (pristine solution) to diluted concentration (5×10^{-6} M solution) for polyynes of different lengths. This can be obtained by normalizing the differences in the concentration of polyynes of different lengths in the pristine and in the diluted solutions over the pristine solution signals. A detailed explanation of the calculations performed is reported in the SI. The largest percentage variation is observed for HC_8H, indicating that lowering the concentration enhances photostability for the shortest polyyne studied. As the sp-carbon chain length increases ($HC_{10}H$), the percentage variation–and thus the stabilizing effect of reduced concentration–decreases. Finally, for $HC_{12}H$ an inversion is observed (i.e., a negative percentage variation), meaning that higher photostability occurs at higher concentration. Figure S4 provides a direct comparison of the photostability of each polyyne at the two concentrations tested.

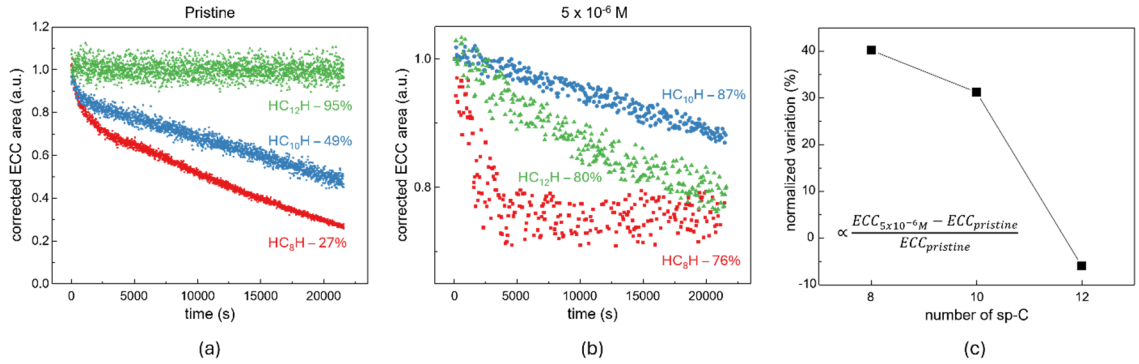

Figure 3. Time-dependent evolution of the SA-corrected Raman ECC area for HC_nH polyynes (n = 8, 10, and 12) under monochromatic synchrotron irradiation. Panels (**a**,**b**) show the results for pristine and 5×10^{-6} M samples, respectively, while panel (**c**) reports the percentage variation in the final ECC values (measured after 6 h of irradiation) between pristine and 5×10^{-6} M samples for each polyyne. The numbers in (**a**,**b**) indicate the percentage of non-photodegraded polyynes after 6 h of irradiation for each species.

The non-trivial photodegradation behavior of polyynes with different lengths can be rationalized by considering the simultaneous occurrence of two competing phenomena. As previously reported in the literature [15,81–83], the chemical structure of polyynes can be altered by the nucleophilic attack of species present in solution or by the solvent itself– i.e., reactions in which electron-rich species chemically attack the electrophilic carbon atoms of the sp-carbon chain via electron donation. It has been demonstrated that, in their excited states, polyynes exhibit a higher π-conjugation along the sp-carbon chain, which leads to a reduction of the HOMO-LUMO gap [84]. Due to the lowered LUMO level of the electrophilic species, the energy barrier associated with the electron transfer from the HOMO of the electron-rich species to the LUMO of the electrophilic one is reduced, thereby facilitating this transfer and the related nucleophilic attack [85]. This implies that this chemical attack is favored when polyynes are excited by photon absorption. Similarly, longer polyynes (i.e., those with higher π-conjugation and, consequently, a reduced HOMO-LUMO gap [16]) are more susceptible to nucleophilic attack, which makes them intrinsically less stable than shorter chains [81,82]. On the other hand, when irradiated with UV light, polyynes can undergo radical formation [86–88]. The stability of the resulting radicals increases with π-conjugation (i.e., with the length of the sp-carbon chain) [89,90]. Consequently, longer polyynes generate more stable radicals, which reduces their tendency to undergo secondary reactions that would otherwise degrade their initial structure, thereby increasing their stability against this degradation pathway. Thus, while short polyynes are more stable against nucleophilic attack, longer ones benefit from the enhanced stability of their radical intermediates. The results shown in Figure 3 suggest that radical formation dominates over nucleophilic attack, as shorter chains are less stable than longer ones under photoexcitation. This competition between radical formation and nucleophilic attack also explains why no clear monotonic trend of photostability with sp-carbon chain length is observed. As a result, the intermediate polyyne ($HC_{10}H$) emerges as the most stable, as it simultaneously benefits from the relative resistance of shorter polyynes to nucleophilic attack and of longer ones to radical-driven degradation.

Similarly, the effect of different terminations on the photodegradation of polyynes was assessed by irradiating sp-carbon chains of the same length (n = 8) but with different terminations: a hydrogen-capped system (HC_8H) and a mono-chlorinated system (HC_8Cl). The time evolution of the Raman ECC peak for these species is reported in Figure 4a. Considering the percentage of non-photodegraded polyynes after 6 h of irradiation (5×10^{-6} M solutions, Figure 4a), HC_8H and HC_8Cl retain 76% and 21% of their initial concentrations, respectively. By comparison, when varying the sp-carbon chain length, the variation in the non-photodegraded polyynes percentage is smaller, with HC_8H, $HC_{10}H$, and $HC_{12}H$ retaining 76%, 87%, and 80% of their initial concentrations, respectively (5×10^{-6} M solutions, Figure 3b). The final percentages of non-photodegraded polyynes for each species in the pristine and 5×10^{-6} M samples are reported in Figure 4b for a better comparison. These results highlight that termination groups play a more significant role than sp-carbon chain length in affecting polyyne photodegradation. This is consistent with previous studies showing that polyynes of different lengths but same terminations exhibit similar photodegradation kinetics [59,91]. Comparing the results for polyynes with different terminations in both pristine and 5×10^{-6} M samples (Figure 4a), it is evident that hydrogenated polyynes are consistently more stable than halogenated ones, regardless of concentration. Specifically, after irradiation of the pristine solutions, the percentages of non-photodegraded polyynes are 27% and 2% for HC_8H and HC_8Cl, respectively. Similarly, for 5×10^{-6} M samples, the percentages are 76% and 21%, respectively. Therefore, the concentration has little effect on the photostability considering different terminations, unlike the case for polyynes of different lengths. As reported in previous work [15], the photostability of polyynes is connected to the bond dissociation energy (BDE) required to break the C–X functional group (X = H or Cl). According to tabulated literature data [92–94], the BDEs are approximately 430 kJ/mol for C–H and 350 kJ/mol for C–Cl, even though small variations are possible depending on the chemical structure of the whole molecule. Since chlorinated polyynes require less energy to break their terminal bonds, they exhibit lower photostability, which explains the faster photodegradation of HC_8Cl compared to HC_8H in all tested samples.

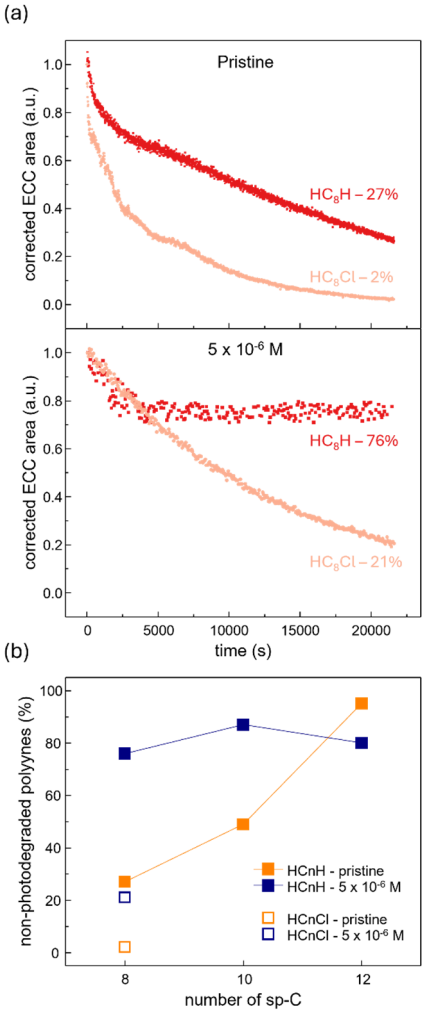

Figure 4. (**a**) Time-dependent evolution of the SA-corrected Raman ECC area for HC_8X polyynes (X = H, Cl) under monochromatic synchrotron irradiation. The panels above and below show the results for pristine and 5 ×

10^{-6} M samples, respectively. The numbers indicate the percentage of non-photodegraded polyynes after 6 h of irradiation for each species. (**b**) Percentages of non-photodegraded polyynes (after 6 h of irradiation) for each species in the pristine and 5×10^{-6} M samples.

We also investigated the photodegradation behavior of polyynes dispersed in different media and in the presence of other nanostructures. Specifically, the pristine monodispersed polyyne solutions were mixed 1:1 (*V*/*V*) with either distilled water or a dispersion of silver nanoparticles (AgNPs) in water. Since the AgNPs are dispersed in water, the polyyne–water mixtures also serve as reference samples to better understand the effect of nanoparticles on polyyne photostability.

Similarly to the previous discussion, the effects of sp-carbon chain length and termination functional groups are considered separately. Figure 5 reports the photostability of pristine polyynes solutions of different sp-carbon chain lengths (HC_nH, n = 8, 10, 12) when mixed with distilled water or with AgNPs. In water, the same trend observed for pristine polyyne solutions (Figure 3a) before mixing with water or AgNPs is maintained, with photostability increasing with sp-carbon chain length. The percentages of non-photodegraded polyynes after irradiation for 7440 s (≈2 h) are 19, 59, and 86% for HC_8H, $HC_{10}H$, and $HC_{12}H$ when mixed with water, respectively. In contrast, in the presence of AgNPs, this trend is completely reversed, with photostability increasing from $HC_{12}H$ (0%) to $HC_{10}H$ (5%) to HC_8H (34%).

Comparing each polyyne across the three environments—pristine solution before mixing, pristine solution mixed with water, and pristine solutions mixed with AgNPs—for each sp-carbon chain length, photodegradation is generally more pronounced in presence of water than in the pristine solution (Figures S5 and 6b). For example, after 7440 s of irradiation, the percentage of non-photodegraded polyynes for HC_8H are 59% and 19% in pristine and water samples, respectively; for $HC_{10}H$ they are 76% and 59%; and for $HC_{12}H$ they are 99% and 86%. The reduced photostability in water can be attributed to its poor compatibility with polyynes [32]. Addition of water can favor degradation pathways such as oxidation [44,45,91], hydrogenation [41,42], and crosslinking due to the lower solubility of non-polar polyynes in a polar solvent like water [32].

Literature studies reports that metal nanoparticles can stabilize polyynes [57,95,96]. Our data partially agrees with these observations: when mixed with AgNPs, HC_8H are more stable than in water alone (non-photodegraded polyynes: 19% in water vs. 34% with AgNPs). However, $HC_{10}H$ and $HC_{12}H$ degrade faster in the presence of AgNPs (59% vs. 5% for $HC_{10}H$, and 86% vs. 0% for $HC_{12}H$ in water and AgNPs, respectively). Differences between previous works, in which an increase in stability is always observed in the presence of nanoparticles, and our results arise from the different experimental approaches. Previous studies exploit surface-enhanced Raman spectroscopy (SERS) using visible excitation sources, where nanoparticles enhance the Raman response of the polyynes closely interacting with nanoparticles. In contrast, we are not performing SERS, as our excitation photon source lies in the UV region, far from the plasmonic resonance of nanoparticles, which in our case is located around 450 nm (Figure S6). Instead, we are tuned to the absorption peaks of each specific polyyne. However, interactions between polyynes and nanoparticles can affect the electronic structure of polyynes (e.g., through charge transfer), thereby shifting their optical gaps and consequently moving them out of the UV resonance [65,97–100]. This implies that, differently from SERS experiments, with UVRR we are not probing polyynes directly interacting with AgNPs, but rather those whose electronic properties remain unaffected, i.e., non-interacting polyynes.

Moreover, the contrasting behavior between shorter (HC_8H) and longer ($HC_{10}H$ and $HC_{12}H$) polyynes, together with the enhanced photostability of shorter sp-carbon chains when mixed with AgNPs, can be rationalized by multiple considerations. First, AgNPs are not fully transparent in the UV region (Figure S6) and absorb part of the incident photons, thereby reducing the power density reaching polyynes and mitigating the photodegradation observed in mixtures with pure water. This shielding effect explains the enhanced photostability of HC_8H in the presence of nanoparticles but does not account for the reduced photostability of $HC_{10}H$ and $HC_{12}H$ compared to water. A second factor must therefore be considered: upon photon absorption, AgNPs can undergo local heating [101–103], exposing nearby polyynes to thermal stresses. Since longer sp-carbon chains are intrinsically less thermally stable [104], they undergo faster degradation, thus possibly explaining the reduced photostability of $HC_{10}H$ and $HC_{12}H$ when mixed with AgNPs compared to when they are mixed with pure water. Taken together, these two effects indicate that when photon shielding prevails (as in HC_8H) photostability is enhanced in the presence of AgNPs, whereas when nanoparticle-mediated degradation such as local heating dominates ($HC_{10}H$ and $HC_{12}H$), photostability is instead reduced.

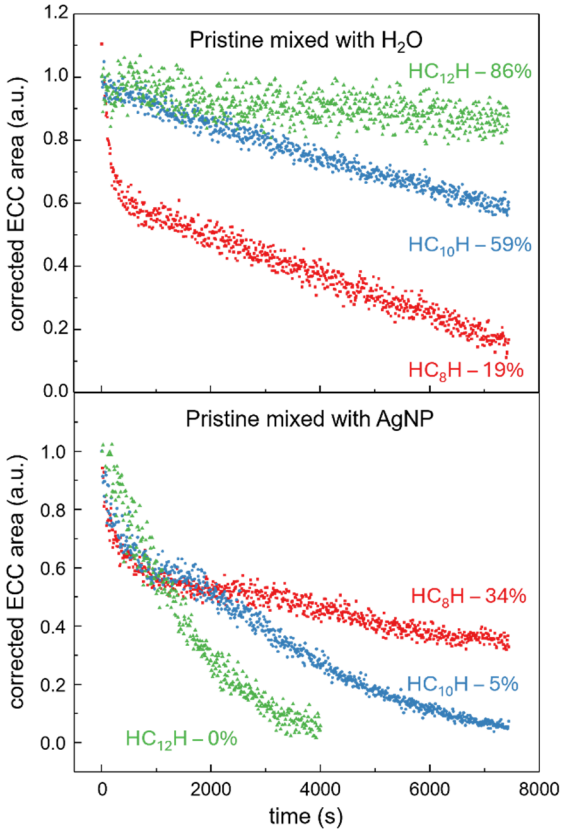

Figure 5. Time-dependent evolution of the SA-corrected Raman ECC area for HC_nH polyynes (n = 8, 10, and 12) under monochromatic synchrotron irradiation. The panels above and below show the results for pristine polyynes solutions mixed 1:1 (*V*/*V*) with pure distilled water and AgNPs in water, respectively. The numbers indicate the percentage of non-photodegraded polyynes after 7440 s of irradiation for each species.

Figure 6a reports the effect of hydrogen and halogen (chlorine) terminations when mixed with water and AgNPs. Both polyynes, whether mixed with distilled water or with AgNPs, exhibit the same trend observed in the pristine samples before mixing with water or AgNPs (Figure 4a), with the chlorinated species degrading faster than their hydrogenated counterparts. As previously discussed, this behavior can be rationalized by the higher bond dissociation energy of the C–H bond compared to C–X (X = halogen; in this case, Cl), which makes hydrogenated polyynes more resistant to photodegradation. Figure S5 shows the photodegradation of HC_8H and HC_8Cl in pristine samples and when mixed with distilled water or AgNPs. The same trends discussed earlier for HC_8H are observed: compared to pristine solutions before mixing with water or AgNPs, polyynes exhibit more pronounced photodegradation in the presence of water due to the low compatibility between polar solvents (water) and polyynes [32] (the percentages of non-photodegraded polyynes are 22% and 4% for HC_8Cl before mixing with water and after mixing, respectively). When AgNPs are added, intermediate photostability is observed (15%), as partial absorption of incident photons reduces the number of photons interacting with the polyynes, partially mitigating the detrimental effect of water. A comparison of the percentages of non-photodegraded polyynes after 7440 s of irradiation for all the tested species, in the pristine solution before mixing and after mixing with either water or AgNPs, is shown in Figure 6b.

These results indicate that addition of water or AgNPs to the pristine solution can either increase or decrease the photostability of polyynes, depending on their structure. The likelihood of an increase or decrease is not strongly influenced by the terminations (polyynes with the same sp-carbon chain length but different terminal groups exhibit the same trend when moving from pristine solution to the addition of pure water and then to AgNPs). Instead, it depends more on the sp-carbon chain length: shorter polyynes are more photostable in the presence of AgNPs than in pure water, whereas longer species undergo greater photodegradation upon the addition of AgNPs.

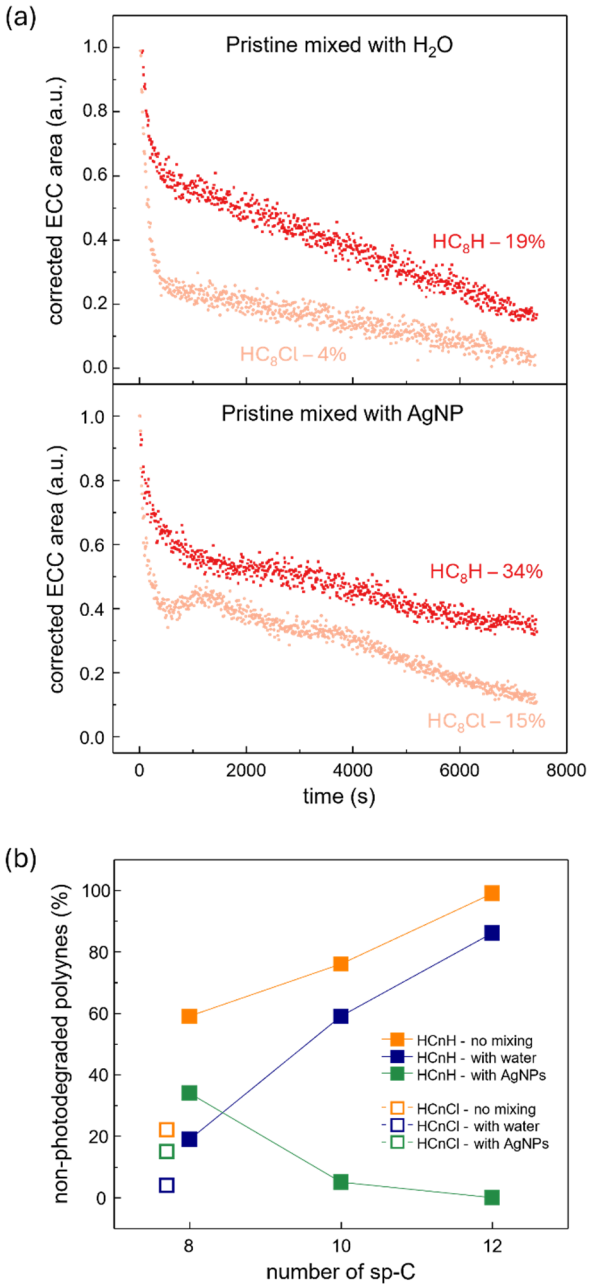

Figure 6. (**a**) Time-dependent evolution of the SA-corrected Raman ECC area for HC_8X polyynes (X = H, Cl) under monochromatic synchrotron irradiation. The panels above and below show the results for pristine polyynes solutions mixed 1:1 (*V*:*V*) with pure distilled water and AgNPs, respectively. The numbers indicate the percentage of non-photodegraded polyynes after 7440 s of irradiation for each species. (**b**) Percentages of non-photodegraded polyynes (after 7440 s of irradiation) for each species in the pristine solution before mixing, the pristine solution mixed with water 1:1 (*V*:*V*), and the pristine solution mixed with AgNPs 1:1 (*V*:*V*).

4. Conclusions

In this work, the photostability of carbon atomic wires with different structures, i.e., sp-carbon chain lengths and termination groups, has been systematically investigated under UV photoexcitation. Unlike previous studies, we employed monodispersed solutions of polyynic wires and exploited UV-tunable synchrotron radiation to selectively photoexcite each species exactly at its main vibronic absorption peak while keeping the delivered power constant. This approach enabled a direct and reliable comparison of the photodegradation behavior of polyynes with different structures. We monitor photodegradation phenomena directly from the time evolution of the Raman spectra of each sample since the excitation wavelengths were in resonance with polyynes' absorption peaks.

By following this strategy, we investigated three hydrogen-terminated polyynes with different lengths (HC_nH, n = 8, 10, 12), revealing a non-trivial dependence of photostability on sp-carbon chain length. Contrary to

the general trend reported in other conditions, HC_8H turned out to be the least stable species, while the intermediate-length wire ($HC_{10}H$) displayed higher photostability. This unexpected behavior can be rationalized by considering the simultaneous occurrence of two competing mechanisms: (i) nucleophilic attack, which becomes more favorable for longer sp-carbon chains, and (ii) photoinduced radical formation, generating less stable radicals in shorter chains. As a result, $HC_{10}H$ represents a balance point, where radical stability is sufficiently high while susceptibility to nucleophilic attack is still relatively low, making it the most stable system.

The role of termination groups was also addressed by comparing hydrogenated and chlorinated CAWs (HC_8X, X = H, Cl). In all cases, hydrogenated species were found to be more stable than their chlorinated counterparts. This difference is explained by considering the bond dissociation energies of the terminal groups: C–H bonds are tighter than C–Cl bonds, making halogenated CAWs more prone to bond cleavage upon photon absorption and thus more sensitive to photodegradation.

When comparing the overall extent of photodegradation after six hours of irradiation, the variation among CAWs of different lengths was relatively small, whereas the difference between hydrogenated and chlorinated terminations was far more pronounced. This indicates that termination groups play a major role in determining polyyne photostability, compared to sp-carbon chain length.

Finally, we investigated environmental effects by dispersing pristine polyyne solutions in distilled water or in aqueous colloidal silver nanoparticles solutions. In water, all polyynes exhibited reduced photostability compared to the pristine solvent, consistent with the poor compatibility of polyynes with polar environments. In the presence of AgNPs, photostability was dictated by the interplay of two competing effects: on one hand, AgNPs absorb UV light, partially shielding polyynes and improving their photostability compared to water alone; on the other hand, AgNPs can promote photodegradation through processes such as local heating. The overall effect depended on the sp-carbon chain length, with shorter polyynes benefiting more from the shielding effect and longer ones being more affected by nanoparticle-induced degradation processes.

In conclusion, these findings provide new insight into the degradation mechanisms of polyynes under light irradiation, highlighting the interplay between intrinsic molecular parameters and environmental factors. The synchrotron-based methodology developed here represents a powerful tool for systematically addressing photostability in sp-carbon systems. The knowledge gained may guide the rational design of polyyne-based materials with improved durability, a crucial step toward their integration in future optoelectronic devices and other nanotechnological applications.

Supplementary Materials

The additional data and information can be downloaded at: https://media.sciltp.com/articles/others/251205100928 7442/PS-25100143-SM-R1.pdf. The supporting information reports additional UV resonance Raman spectra, UV-Vis spectra, time evolution of polyynes under photoirradiation, and the models used to correct self-absorption and to evaluate the percentage variation from pristine to diluted solutions for each polyyne.

Author Contributions

S.M., P.M., V.R., A.L.B., C.E.B. and C.S.C. planned and conceptualized the work. S.M., P.M., B.R., V.R. and C.S.C. carried out UV resonance measurements. S.M. and P.M. performed data analysis. S.M. wrote the first version of the paper. All authors contributed to the data discussion. All authors have read and agreed to the published version of the manuscript.

Funding

S.M., P.M., V.R. A.L.B. and C.S.C. acknowledge funding from the European Research Council (ERC) under the European Union's Horizon 2020 research and innovation program ERC Consolidator Grant (ERC CoG2016 EspLORE grant agreement No. 724610, website: www.esplore.polimi.it accessed on 1 October 2025). C.S.C. acknowledges funding by Project funded under the National Recovery and Resilience Plan (NRRP), Mission 4 Component 2 Investment 1.3–Call for tender No. 1561 of 11.10.2022 of Ministero dell'Università e della Ricerca (MIUR); funded by the European Union−NextGenerationEU. Award Number: Project code PE0000021, Concession Decree No. 1561 of 11.10.2022 adopted by Ministero dell'Università e della Ricerca (MIUR), CUP D43C22003090001, Project title "Network 4 Energy Sustainable Transition−NEST". The authors acknowledge the CERIC-ERIC Consortium for the access to experimental facilities and financial support (proposal number 20227204).

Institutional Review Board Statement

Not applicable.

Informed Consent Statement

Not applicable.

Data Availability Statement

The data that support the findings of this study are available from the corresponding author upon reasonable request. They have been deposited in Zenodo with this identifier https://doi.org/10.5281/zenodo.17818276.

Conflicts of Interest

The authors declare no conflict of interest.

Use of AI and AI-Assisted Technologies

No AI tools were utilized for this paper.

References

1. Casari, C.S.; Tommasini, M.; Tykwinski, R.R.; et al. Carbon-atom wires: 1-D systems with tunable properties. *Nanoscale* **2016**, *8*, 4414–4435.
2. Casari, C.S.; Milani, A. Carbyne: From the elusive allotrope to stable carbon atom wires. *MRS Commun.* **2018**, *8*, 207–219.
3. Ghosh, S.; Righi, M.; Melesi, S.; et al. Cumulenic sp-Carbon atomic wires wrapped with polymer for supercapacitor application. *Carbon* **2025**, *234*, 119952. https://doi.org/10.1016/j.carbon.2024.119952.
4. Bettini, L.G.; Della Foglia, F.; Piseri, P.; et al. Interfacial properties of a carbyne-rich nanostructured carbon thin film in ionic liquid. *Nanotechnology* **2016**, *27*, 115403.
5. Zhang, D.; Yang, Z.; Li, X.; et al. Synthesis of an Sp-Carbon-Rich Carbonaceous Material Exhibiting Distinctive Anode Performance. *Angew. Chem. Int. Ed.* **2025**, *64*, e202514245. https://doi.org/10.1002/anie.202514245.
6. Anikina, E.; Banerjee, A.; Beskachko, V.; et al. Li-decorated carbyne for hydrogen storage: Charge induced polarization and van't Hoff hydrogen desorption temperature. *Sustain. Energy Fuels* **2020**, *4*, 691–699.
7. Sorokin, P.B.; Lee, H.; Antipina, L.Y.; et al. Calcium-decorated carbyne networks as hydrogen storage media. *Nano Lett.* **2011**, *11*, 2660–2665.
8. Scaccabarozzi, A.D.; Milani, A.; Peggiani, S.; et al. A field-effect transistor based on cumulenic sp-carbon atomic wires. *J. Phys. Chem. Lett.* **2020**, *11*, 1970–1974.
9. Pecorario, S.; Scaccabarozzi, A.D.; Fazzi, D.; et al. Stable and Solution-Processable Cumulenic sp-Carbon Wires: A New Paradigm for Organic Electronics. *Adv. Mater.* **2022**, *34*, 2110468.
10. Hu, F.; Zeng, C.; Long, R.; et al. Supermultiplexed optical imaging and barcoding with engineered polyynes. *Nat. Methods* **2018**, *15*, 194–200.
11. Castiglioni, C.; Tommasini, M.; Zerbi, G. Raman spectroscopy of polyconjugated molecules and materials: Confinement effect in one and two dimensions. *Philos. Trans. R. Soc. Lond. Ser. A Math. Phys. Eng. Sci.* **2004**, *362*, 2425–2459. https://doi.org/10.1098/rsta.2004.1448.
12. Tommasini, M.; Fazzi, D.; Milani, A.; et al. Intramolecular Vibrational Force Fields for Linear Carbon Chains through an Adaptative Linear Scaling Scheme. *J. Phys. Chem. A* **2007**, *111*, 11645–11651. https://doi.org/10.1021/jp0757006.
13. Yang, S.; Kertesz, M.; Zólyomi, V.; et al. Application of a Novel Linear/Exponential Hybrid Force Field Scaling Scheme to the Longitudinal Raman Active Mode of Polyyne. *J. Phys. Chem. A* **2007**, *111*, 2434–2441. https://doi.org/10.1021/jp067866x.
14. Yang, S.; Kertesz, M. Linear Cn Clusters: Are They Acetylenic or Cumulenic? *J. Phys. Chem. A* **2008**, *112*, 146–151. https://doi.org/10.1021/jp076805b.
15. Melesi, S.; Pińkowski, P.; Pigulski, B.; et al. Probing the Stability of Halogenated Carbon Atomic Wires in Electrospun Nanofibers via Raman Spectroscopy. *J. Phys. Chem. C* **2025**, *129*, 12916–12926. https://doi.org/10.1021/acs.jpcc.5c02960.
16. Melesi, S.; Marabotti, P.; Milani, A.; et al. Impact of Halogen Termination and Chain Length on π-Electron Conjugation and Vibrational Properties of Halogen-Terminated Polyynes. *J. Phys. Chem. A* **2024**, *128*, 2703–2716.
17. Chalifoux, W.A.; Tykwinski, R.R. Synthesis of extended polyynes: Toward carbyne. *Comptes Rendus Chim.* **2009**, *12*, 341–358.
18. Kudryavtsev, Y.U.P. Syntheses of carbyne and carbynoid structures. *Carbyne Carbynoid Struct.* **1999**, *21*, 39.

19. Szafert, S.; Gladysz, J.A. Carbon in One Dimension: Structural Analysis of the Higher Conjugated Polyynes. *Chem. Rev.* **2003**, *103*, 4175–4206. https://doi.org/10.1021/cr030041o.
20. Chalifoux, W.A.; Tykwinski, R.R. Synthesis of polyynes to model the sp-carbon allotrope carbyne. *Nat. Chem.* **2010**, *2*, 967–971. https://doi.org/10.1038/nchem.828.
21. Tykwinski, R.R.; Chalifoux, W.; Eisler, S.; et al. Toward carbyne: Synthesis and stability of really long polyynes. *Pure Appl. Chem.* **2010**, *82*, 891–904.
22. Kroto, H.W.; Heath, J.R.; O'Brien, S.C.; et al. C60: Buckminsterfullerene. *Nature* **1985**, *318,* 162–163. https://doi.org/10.1038/318162a0.
23. Milani, P.; Iannotta, S. *Cluster Beam Synthesis of Nanostructured Materials*; Springer Science & Business Media: Berlin, Germany, 2012.
24. Ravagnan, L.; Siviero, F.; Lenardi, C.; et al. Cluster-Beam Deposition and in situ Characterization of Carbyne-Rich Carbon Films. *Phys. Rev. Lett.* **2002**, *89*, 285506. https://doi.org/10.1103/PhysRevLett.89.285506.
25. Casari, C.S.; Giannuzzi, C.S.; Russo, V. Carbon-atom wires produced by nanosecond pulsed laser deposition in a background gas. *Carbon* **2016**, *104*, 190–195.
26. Matsutani, R.; Inoue, K.; Sanada, T.; et al. Preparation of long-chain polyynes of C28H2 and C30H2 by liquid-phase laser ablation. *J. Photochem. Photobiol. A Chem.* **2012**, *240*, 1–4.
27. Marabotti, P.; Peggiani, S.; Vidale, A.; et al. Pulsed laser ablation in liquid of sp-carbon chains: Status and recent advances. *Chin. Phys. B* **2022**, *31*, 125202.
28. Tsuji, M.; Kuboyama, S.; Matsuzaki, T.; et al. Formation of hydrogen-capped polyynes by laser ablation of C60 particles suspended in solution. *Carbon* **2003**, *41*, 2141–2148.
29. Compagnini, G.; Mita, V.; Cataliotti, R.S.; et al. Short polyyne chains produced by pulsed laser ablation of graphite in water. *Carbon* **2007**, *45*, 2456–2458.
30. Sato, Y.; Kodama, T.; Shiromaru, H.; et al. Synthesis of polyyne molecules from hexane by irradiation of intense femtosecond laser pulses. *Carbon* **2010**, *48*, 1673–1676. https://doi.org/10.1016/j.carbon.2009.12.036.
31. Hu, A.; Sanderson, J.; Zaidi, A.A.; et al. Direct synthesis of polyyne molecules in acetone by dissociation using femtosecond laser irradiation. *Carbon* **2008**, *46*, 1823–1825. https://doi.org/10.1016/j.carbon.2008.07.036.
32. Peggiani, S.; Marabotti, P.; Lotti, R.A.; et al. Solvent-dependent termination, size and stability in polyynes synthesized via laser ablation in liquids. *Phys. Chem. Chem. Phys.* **2020**, *22*, 26312–26321.
33. Peggiani, S.; Facibeni, A.; Milani, A.; et al. In situ synthesis of polyynes in a polymer matrix via pulsed laser ablation in a liquid. *Mater. Adv.* **2020**, *1*, 2729–2736.
34. Park, Y.E.; Shin, S.K.; Park, S.M. The physical effects on the formation of polyynes by laser ablation. *Chem. Phys. Lett.* **2013**, *568–569*, 112–116. https://doi.org/10.1016/j.cplett.2013.03.016.
35. Matsutani, R.; Kakimoto, T.; Tanaka, H.; et al. Preparation of polyynes by liquid-phase laser ablation using different irradiation target materials and solvents. *Carbon* **2011**, *49*, 77–81. https://doi.org/10.1016/j.carbon.2010.08.044.
36. Marabotti, P.; Peggiani, S.; Melesi, S.; et al. Exploring the Growth Dynamics of Size-Selected Carbon Atomic Wires with In Situ UV Resonance Raman Spectroscopy. *Small* **2024**, *20*, 2403054.
37. Peggiani, S.; Facibeni, A.; Marabotti, P.; et al. A single liquid chromatography procedure to concentrate, separate and collect size-selected polyynes produced by pulsed laser ablation in water. *Fuller. Nanotub. Carbon Nanostructures* **2023**, *31*, 224–230. https://doi.org/10.1080/1536383X.2022.2137498.
38. Wakabayashi, T.; Saikawa, M.; Wada, Y.; et al. Isotope scrambling in the formation of cyanopolyynes by laser ablation of carbon particles in liquid acetonitrile. *Carbon* **2012**, *50*, 47–56.
39. Wakabayashi, T.; Szczepaniak, U.; Tanaka, K.; et al. Phosphorescence of hydrogen-capped linear polyyne molecules C8H2, C10H2 and C12H2 in solid hexane matrices at 20 K. *Photochem* **2022**, *2*, 181–201.
40. Casari, C.S.; Bassi, A.L.; Ravagnan, L.; et al. Chemical and thermal stability of carbyne-like structures in cluster-assembled carbon films. *Phys. Rev. B* **2004**, *69*, 075422.
41. Cataldo, F. Synthesis of polyynes in a submerged electric arc in organic solvents. *Carbon* **2004**, *42*, 129–142.
42. Cataldo, F. Storage stability of polyynes and cyanopolyynes in solution and the effect of ammonia or hydrochloric acid. *Fuller. Nanotub. Carbon Nanostructures* **2007**, *15*, 155–166.
43. Cataldo, F. Polyynes production in a solvent-submerged electric arc between graphite electrodes. III. Chemical reactivity and stability toward air, ozone, and light. *Fuller. Nanotub. Carbon Nanostructures* **2004**, *12*, 633–646. https://doi.org/10.1081/FST-200026951.
44. Cataldo, F. Stability of polyynes in air and their degradation by ozonolysis. *Polym. Degrad. Stab.* **2006**, *91*, 317–323.
45. Cui, W.; Saito, T.; Ayala, P.; et al. Oxidation stability of confined linear carbon chains, carbon nanotubes, and graphene nanoribbons as 1D nanocarbons. *Nanoscale* **2019**, *11*, 15253–15258. https://doi.org/10.1039/C9NR04924J.

46. Rivelino, R.; Santos, R.B.D.; de Brito Mota, F.; et al. Conformational effects on structure, electron states, and Raman scattering properties of linear carbon chains terminated by graphene-like pieces. *J. Phys. Chem. C* **2010**, *114*, 16367–16372.
47. Cataldo, F.; Ursini, O.; Milani, A.; et al. One-pot synthesis and characterization of polyynes end-capped by biphenyl groups (α,ω-biphenylpolyynes). *Carbon* **2018**, *126*, 232–240. https://doi.org/10.1016/j.carbon.2017.09.098.
48. Arora, A.; Baksi, S.D.; Weisbach, N.; et al. Monodisperse Molecular Models for the sp Carbon Allotrope Carbyne; Syntheses, Structures, and Properties of Diplatinum Polyynediyl Complexes with PtC20Pt to PtC52Pt Linkages. *ACS Cent. Sci.* **2023**, *9*, 2225–2240.
49. Pigulski, B.; Jarszak, A.; Szafert, S. Selective synthesis of iridium (iii) end-capped polyynes by oxidative addition of 1-iodopolyynes to Vaska's complex. *Dalton Trans.* **2018**, *47*, 17046–17054.
50. Gulia, N.; Pigulski, B.; Szafert, S. Palladium End-Capped Polyynes via Oxidative Addition of 1-Haloalkynes to $Pd(PPh_3)_4$. *Organometallics* **2015**, *34*, 673–682.
51. Matsutani, R.; Ozaki, F.; Yamamoto, R.; et al. Preparation of polyynes up to C22H2 by liquid-phase laser ablation and their immobilization into SiO_2 gel. *Carbon* **2009**, *47*, 1659–1663.
52. Shi, L.; Rohringer, P.; Suenaga, K.; et al. Confined linear carbon chains as a route to bulk carbyne. *Nat. Mater.* **2016**, *15*, 634–639. https://doi.org/10.1038/nmat4617.
53. Nishide, D.; Dohi, H.; Wakabayashi, T.; et al. Single-wall carbon nanotubes encaging linear chain C10H2 polyyne molecules inside. *Chem. Phys. Lett.* **2006**, *428*, 356–360. https://doi.org/10.1016/j.cplett.2006.07.016.
54. Zhang, Y.; Zhao, J.; Fang, Y.; et al. Preparation of long linear carbon chain inside multi-walled carbon nanotubes by cooling enhanced hydrogen arc discharge method. *Nanoscale* **2018**, *10*, 17824–17833. https://doi.org/10.1039/C8NR05465G.
55. Okada, S.; Fujii, M.; Hayashi, S. Immobilization of polyynes adsorbed on Ag nanoparticle aggregates into poly (vinyl alcohol) films. *Carbon* **2011**, *49*, 4704–4709.
56. An, K.; Wei, G.; Qi, G.; et al. Stability improvement of C_8H_2 and $C_{10}H_2$ embedded in poly (vinyl alcohol) films with adsorption on gold nanoparticles. *Chem. Phys. Lett.* **2015**, *637*, 71–76.
57. Casari, C.S.; Russo, V.; Bassi, A.L.; et al. Stabilization of linear carbon structures in a solid Ag nanoparticle assembly. *Appl. Phys. Lett.* **2007**, *90*, 013111.
58. Kabaciński, P.; Marabotti, P.; Fazzi, D.; et al. Disclosing Early Excited State Relaxation Events in Prototypical Linear Carbon Chains. *J. Am. Chem. Soc.* **2023**, *145*, 18382–18390. https://doi.org/10.1021/jacs.3c04163.
59. Cataldo, F.; Strazzulla, G.; Iglesias-Groth, S. UV photolysis of polyynes at $\lambda = 254$ nm and at $\lambda > 222$ nm. *Int. J. Astrobiol.* **2008**, *7*, 107–116.
60. Lee, P.C.; Meisel, D. Adsorption and surface-enhanced Raman of dyes on silver and gold sols. *J. Phys. Chem.* **1982**, *86*, 3391–3395.
61. Amirjani, A.; Firouzi, F.; Haghshenas, D.F. Predicting the size of silver nanoparticles from their optical properties. *Plasmonics* **2020**, *15*, 1077–1082.
62. D'Amico, F.; Saito, M.; Bencivenga, F.; et al. UV resonant Raman scattering facility at Elettra. *Nucl. Instrum. Methods Phys. Res. A* **2013**, *703*, 33–37. https://doi.org/10.1016/j.nima.2012.11.037.
63. Inoue, K.; Matsutani, R.; Sanada, T.; et al. Preparation of long-chain polyynes of C24H2 and C26H2 by liquid-phase laser ablation in decalin. *Carbon* **2010**, *48*, 4209–4211. https://doi.org/10.1016/j.carbon.2010.07.020.
64. Milani, A.; Tommasini, M.; Barbieri, V.; et al. Semiconductor-to-metal transition in carbon-atom wires driven by sp^2 conjugated end groups. *J. Phys. Chem. C* **2017**, *121*, 10562–10570.
65. Milani, A.; Barbieri, V.; Facibeni, A.; et al. Structure modulated charge transfer in carbon atomic wires. *Sci. Rep.* **2019**, *9*, 1648.
66. Gao, Y.; Hou, Y.; Gamez, F.G.; et al. The loss of endgroup effects in long pyridyl-endcapped oligoynes on the way to carbyne. *Nat. Chem.* **2020**, *12*, 1143–1149.
67. Milani, A.; Tommasini, M.; Russo, V.; et al. Raman spectroscopy as a tool to investigate the structure and electronic properties of carbon-atom wires. *Beilstein J. Nanotechnol.* **2015**, *6*, 480–491.
68. Tabata, H.; Fujii, M.; Hayashi, S.; et al. Raman and surface-enhanced Raman scattering of a series of size-separated polyynes. *Carbon* **2006**, *44*, 3168–3176.
69. Tommasini, M.; Milani, A.; Fazzi, D.; et al. π-Conjugation and End Group Effects in Long Cumulenes: Raman Spectroscopy and DFT Calculations. *J. Phys. Chem. C* **2014**, *118*, 26415–26425. https://doi.org/10.1021/jp509724d.
70. Lee, S.; Heller, E.J. Time-dependent theory of Raman scattering. *J. Chem. Phys.* **1979**, *71*, 4777–4788. https://doi.org/10.1063/1.438316.
71. Albrecht, A.C. On the Theory of Raman Intensities. *J. Chem. Phys.* **1961**, *34*, 1476–1484. https://doi.org/10.1063/1.1701032.
72. Marabotti, P.; Tommasini, M.; Castiglioni, C.; et al. Electron-phonon coupling and vibrational properties of size-selected linear carbon chains by resonance Raman scattering. *Nat. Commun.* **2022**, *13*, 5052.

73. Marabotti, P.; Tommasini, M.; Castiglioni, C.; et al. Synchrotron-based UV resonance Raman spectroscopy probes size confinement, termination effects, and anharmonicity of carbon atomic wires. *Carbon* **2024**, *216*, 118503. https://doi.org/10.1016/j.carbon.2023.118503.
74. Asher, S.A. UV resonance Raman studies of molecular structure and dynamics. *Annu. Rev. Phys. Chem.* **1988**, *39*, 537–588.
75. Ludwig, M.; Asher, S.A. Self-Absorption in Resonance Raman and Rayleigh Scattering: A Numerical Solution. *Appl. Spectrosc.* **1988**, *42*, 1458–1466. https://doi.org/10.1366/0003702884429670.
76. Hong, Z.; Asher, S.A. Dependence of Raman and Resonance Raman Intensities on Sample Self-Absorption. *Appl. Spectrosc.* **2015**, *69*, 75–83. https://doi.org/10.1366/14-07531.
77. Peggiani, S.; Marabotti, P.; Lotti, R.A.; et al. Solvent-dependent termination, size and stability in polyynes synthesized via laser ablation in liquid. *Phys. Chem. Chem. Phys.* **2020**, *22*, 26312–26321. https://doi.org/10.1039/D0CP04132G.
78. Cataldo, F.; Ursini, O.; Angelini, G. Kinetics of polyynes formation with the submerged carbon arc. *J. Electroanal. Chem.* **2007**, *602*, 82–90.
79. Ye, C.; Gray, V.; Mårtensson, J.; et al. Annihilation versus excimer formation by the triplet pair in triplet–triplet annihilation photon upconversion. *J. Am. Chem. Soc.* **2019**, *141*, 9578–9584.
80. Hoche, J.; Schmitt, H.-C.; Humeniuk, A.; et al. The mechanism of excimer formation: An experimental and theoretical study on the pyrene dimer. *Phys. Chem. Chem. Phys.* **2017**, *19*, 25002–25015. https://doi.org/10.1039/C7CP03990E.
81. Pigulski, B.; Gulia, N.; Szafert, S. Reactivity of Polyynes: Complex Molecules from Simple Carbon Rods. *Eur. J. Org. Chem.* **2019**, *2019*, 1420–1445. https://doi.org/10.1002/ejoc.201801350.
82. Chalifoux, W.A.; Tykwinski, R.R. Oligoynes and polyynes. *Can. J. Chem.* **2025**. https://doi.org/10.1139/cjc-2025-0069.
83. Yosipof, A.; Basch, H.; Hoz, S. Nucleophilic and Electrophilic Reactions of Polyynes Catalyzed by an Electric Field: Toward Barcoding of Carbon Nanotubes Like Long Homogeneous Substrates. *J. Phys. Chem. A* **2013**, *117*, 5023–5027. https://doi.org/10.1021/jp402758u.
84. Movsisyan, L.D.; Peeks, M.D.; Greetham, G.M.; et al. Photophysics of Threaded sp-Carbon Chains: The Polyyne is a Sink for Singlet and Triplet Excitation. *J. Am. Chem. Soc.* **2014**, *136*, 17996–18008. https://doi.org/10.1021/ja510663z.
85. Walvoord, R.R.; Huynh, P.N.H.; Kozlowski, M.C. Quantification of Electrophilic Activation by Hydrogen-Bonding Organocatalysts. *J. Am. Chem. Soc.* **2014**, *136*, 16055–16065. https://doi.org/10.1021/ja5086244.
86. Zelikoff, M.; Aschenbrand, L.M. Vacuum Ultraviolet Photochemistry. Part III. Acetylene a 1849 A. *J. Chem. Phys.* **1956**, *24*, 1034–1037. https://doi.org/10.1063/1.1742673.
87. Glicker, S.; Okabe, H. Photochemistry of diacetylene. *J. Phys. Chem.* **1987**, *91*, 437–440.
88. Cataldo, F. A study on ethylene and acetylene photoligomerization and photopolymerization. *J. Photochem. Photobiol. A Chem.* **1996**, *99*, 75–81. https://doi.org/10.1016/1010-6030(96)04356-0.
89. Tang, B.; Zhao, J.; Xu, J.-F.; et al. Tuning the stability of organic radicals: From covalent approaches to non-covalent approaches. *Chem. Sci.* **2020**, *11*, 1192–1204. https://doi.org/10.1039/C9SC06143F.
90. Velloth, A.; Kumar, P.; Butt, S.; et al. C–Centered Radicals: Generation, Detection, Stability and Perspectives. *Asian J. Org. Chem.* **2025**, *14*, e202400686. https://doi.org/10.1002/ajoc.202400686.
91. Cataldo, F. Polyynes production in a solvent-submerged electric arc between graphite electrodes. III. chemical reactivity and stability toward air, ozone, and light. *Fuller. Nanotub. Carbon Nanostructures* **2004**, *12*, 633–646.
92. McGivern, W.S.; Derecskei-Kovacs, A.; North, S.W.; et al. Computationally Efficient Methodology to Calculate C−H and C−X (X = F, Cl, and Br) Bond Dissociation Energies in Haloalkanes. *J. Phys. Chem. A* **2000**, *104*, 436–442. https://doi.org/10.1021/jp993275d.
93. Cioslowski, J.; Liu, G.; Moncrieff, D. Thermochemistry of Homolytic C−C, C−H, and C−Cl Bond Dissociations in Polychloroethanes: Benchmark Electronic Structure Calculations. *J. Am. Chem. Soc.* **1997**, *119*, 11452–11457. https://doi.org/10.1021/ja971108q.
94. Vollhardt, K.P.C.; Schore, N.E. *Organic Chemistry: Structure and Function*; Macmillan: London, UK, 2003.
95. Kim, H.; Tarakeshwar, P.; Fujikado, N.M.; et al. Pseudocarbynes: Linear carbon chains stabilized by metal clusters. *J. Phys. Chem. C* **2020**, *124*, 19355–19361.
96. Marabotti, P.; Peggiani, S.; Facibeni, A.; et al. In situ surface-enhanced Raman spectroscopy to investigate polyyne formation during pulsed laser ablation in liquid. *Carbon* **2022**, *189*, 219–229. https://doi.org/10.1016/j.carbon.2021.12.060.
97. Milani, A.; Lucotti, A.; Russo, V.; et al. Charge transfer and vibrational structure of sp-hybridized carbon atomic wires probed by surface enhanced Raman spectroscopy. *J. Phys. Chem. C* **2011**, *115*, 12836–12843.
98. Lucotti, A.; Casari, C.S.; Tommasini, M.; et al. sp Carbon chain interaction with silver nanoparticles probed by Surface Enhanced Raman Scattering. *Chem. Phys. Lett.* **2009**, *478*, 45–50. https://doi.org/10.1016/j.cplett.2009.06.030.
99. Condorelli, M.; Speciale, A.; Cimino, F.; et al. Nano-hybrid Au@ LCCs systems displaying anti-inflammatory activity. *Materials* **2022**, *15*, 3701.
100. Grasso, G.; D'Urso, L.; Messina, E.; et al. A mass spectrometry and surface enhanced Raman spectroscopy study of the interaction between linear carbon chains and noble metals. *Carbon* **2009**, *47*, 2611–2619.

101. Zhu, H.; Gablech, E.; Gablech, I.; et al. The collective photothermal effect of silver nanoparticles probed by a microbolometer. *Commun. Mater.* **2024**, *5*, 66. https://doi.org/10.1038/s43246-024-00509-0.
102. Anuthum, S.; Hasegawa, F.; Lertvachirapaiboon, C.; et al. Plasmonic photothermal properties of silver nanoparticle grating films. *Phys. Chem. Chem. Phys.* **2022**, *24*, 7060–7067. https://doi.org/10.1039/D1CP05893B.
103. Huang, H.; Sivayoganathan, M.; Duley, W.W.; et al. Efficient localized heating of silver nanoparticles by low-fluence femtosecond laser pulses. *Appl. Surf. Sci.* **2015**, *331*, 392–398. https://doi.org/10.1016/j.apsusc.2015.01.086.
104. Movsisyan, L.D.; Franz, M.; Hampel, F.; et al. Polyyne Rotaxanes: Stabilization by Encapsulation. *J. Am. Chem. Soc.* **2016**, *138*, 1366–1376. https://doi.org/10.1021/jacs.5b12049.